Journal of Catalysis **209,** 417–426 (2002)
doi:10.1006/jcat.2002.3644

# Effect of Preparation Method and Redox Treatment on the Reducibility and Structure of Supported Ceria–Zirconia Mixed Oxide

Alexander I. Kozlov,* Do Heui Kim,* Aleksey Yezerets,*,[1] Paul Andersen,†
Harold H. Kung,* and Mayfair C. Kung*,[2]

*Department of Chemical Engineering, Northwestern University, Evanston, Illinois 60208-3120; and †Johnson Matthey Catalytic Systems Division, 436 Devon Park Drive, Wayne, Pennsylvania 19087

Received December 7, 2001; revised April 17, 2002; accepted April 23, 2002

**An $Al_2O_3$-supported $Ce_{0.45}Zr_{0.55}O_2$ was prepared with a modified sol–gel procedure designed to maximize the interaction between ceria and zirconia and promote thermal stability of alumina. Its properties, characterized in detail with XRD, TPR, and laser Raman spectroscopy, were compared with those of more conventional preparations. This sample consisted of finely dispersed $Ce_xZr_{1-x}O_2$ and had a high fraction of easily reducible $Ce^{4+}$. Complete insertion of Zr into the ceria fluorite structure was observed after 900°C oxidation. After reduction at 980°C and reoxidation at 900°C, the mixed oxide particles remained small and furthermore still remained single phase and homogeneous by XRD characterization. Redox treatment enhanced the reducibility of $Ce^{4+}$ in this sample. One feature of the enhancement, similar to that in bulk mixed oxide of similar composition, was an increase in the ratio of $Ce^{4+}$ that was reducible at ∼491°C relative to the ones at ∼577°C. A new low-temperature reduction feature appeared at 320°C. This was attributed to the segregation of a small fraction of $Ce^{3+}$ from the mixed oxide upon reduction and the subsequent formation of a finely dispersed ceria-rich phase on the surface of mixed oxide crystallites upon reoxidation. This phenomenon was particular to the supported samples because $Al_2O_3$ was able to stabilize the particle size of the mixed oxide during severe redox and thermal treatments.** © 2002 Elsevier Science (USA)

*Key Words:* **ceria–zirconia mixed oxides; oxygen storage capacity; three-way catalysts; sol–gel preparation; structural and redox properties.**

## 1. INTRODUCTION

Three-way catalysts operate under an atmosphere that oscillates between rich and lean conditions. An oxygen storage component in the form of ceria-containing oxide is included in the catalyst formulation to moderate the effect of such oscillations on the catalytic performance (1–3). The major problem with $CeO_2$ is the loss of oxygen storage capacity (OSC) due to reduction of surface area upon thermal treatment (4, 5). The advent of $Ce_xZr_{1-x}O_2$ as the new generation of oxygen storage component ushers in a step change in the catalytic performance. Insertion of $ZrO_2$ into the cubic $CeO_2$ results in increased thermal stability (6). Distortion of the $O^{2-}$ sublattice in the mixed oxide permits a higher mobility of the lattice oxygen (7–9) and reduction is no longer confined to the surface but extends deep into the bulk (4, 10). The composition of the binary oxide impacts the OSC. It is observed that the percentage of reducible $Ce^{4+}$ and the thermal stability increased with Zr/Ce ratio. On the other hand, at low Zr content, the binary oxide is of the cubic phase, which is favorable for high oxygen mobility. In the intermediate composition range, phase segregation occurs (11), and at even higher Zr content the stable phases are tetragonal and monoclinic. Nunan and Bortun (12) reported that the phase segregation could be deterred by doping the mixed oxide with yttrium. After severe aging, this ternary mixed oxide has higher OSC than a $Ce^{4+}$-rich mixed oxide. Another method of stabilization of the cubic phase at intermediate composition was to decrease the particle size of the mixed oxide (4).

A new phenomenon associated with $Ce_xZr_{1-x}O_2$ is improved low-temperature reducibility of the oxide by a deep reduction and mild oxidation treatment (4, 13–16). In contrast, the same treatment of bulk $CeO_2$ results in a total loss of low-temperature $H_2$ uptake (4). This enhancement in reducibility is not observed for all bulk $Ce_xZr_{1-x}O_2$ but depends strongly on the preparatory method (6, 17). Even in the extensively studied preparations produced by Rhodia, the enhancement is only pronounced after thermal sintering of the fresh samples (13, 14). In addition, the improvement in reducibility is also highly dependent on the composition of the mixed oxide (14). The origin of this phenomenon is not well understood. Fally *et al.* suggested that the improved reducibility of the mixed oxide upon redox aging originated from structural changes in the nanoscale (16).

Although bulk $Ce_xZr_{1-x}O_2$ mixed oxides have been studied extensively, its supported form on $Al_2O_3$ has not received much attention (5, 18, 19). In earlier work where

[1] Present address: Cummins, Inc., 1900 McKinley Avenue, Columbus, IN 47201.

[2] To whom correspondence should be addressed. Fax: 1- (847) 467-1018. E-mail: m-kung@northwestern.edu.



0021-9517/02 $35.00

ceria was used as the oxygen storage component, formation of $CeAlO_3$ was of concern because this leads to a loss in the OSC (20, 21). The tendency to form $CeAlO_3$ is greatly suppressed for the supported $Ce_xZr_{1-x}O_2$ (19, 22, 23) and only occurs for high-Zr-content preparations after undergoing severe thermal aging and reduction (23). An added benefit of the presence of alumina is its ability to stabilize the nanostructure of $Ce_xZr_{1-x}O_2$ (19, 22, 23), with the smallest particle $Ce_xZr_{1-x}O_2$ being that with the highest Zr content. Most of the $Ce_xZr_{1-x}O_2/Al_2O_3$ reported is prepared by coimpregnation of salt solution containing $Ce^{3+}$ and $Zr^{4+}$ onto alumina. Generally, this method results in incomplete incorporation of Zr, and phase and compositional separation after aging for intermediate compositions.

Thus, results to date indicate the benefits of higher-Zr-content mixed oxides and the difficulty of maintaining these oxides in a single cubic phase upon thermal treatment. The existence of metastable phases of $Ce_xZr_{1-x}O_2$ (24–26) in addition to the stable thermodynamic ones, and the sensitivity of the stability of these metastable phases to the particle size, suggests that the synthesis method could be of critical importance to the OSC of the mixed oxide (27). The benefits of including alumina in the catalyst formulation is enormous, yet the same problem of phase segregation occurs at intermediate compositions and not much attention has been focused on modifying the conventional coimpregnation method to obtain more stable and homogeneous preparations. Thus a major emphasis of this study is to evaluate the effect of different synthesis methods on the redox property of $CeO_2$–$ZrO_2$–$Al_2O_3$. Related to the importance of the preparation method is the observation that enhanced reducibility after redox cycling is only present in bulk oxides using certain preparation methods. Since similar changes in temperature and composition of the exhaust atmosphere take place in transient driving cycles, it is of practical interest to further understand this phenomenon and relate it to the synthesis variables used in the preparation of $CeO_2$–$ZrO_2$–$Al_2O_3$.

## 2. EXPERIMENTAL

### 2.1. Sample Preparation

$Al_2O_3$ support (267 $m^2/g$) was prepared by hydrolyzing aluminum isopropoxide (Aldrich, 99.99%) in the presence of the chelating agent, 2-methyl-2,4-pentanediol (Aldrich, 99%), using a procedure similar to that described by Maeda *et al.* (28). After aging for 14 h at 90°C, the sample was heated in flowing air at 1°/min to 700°C and held at this temperature for 2 h. $H_2O$ (2%) was introduced into the air flow at 500°C and the concentration was increased to 6% at 700°C (29). The resulting $Al_2O_3$ was used to prepare all the samples studied. Its BET area was 267 $m^2/g$.

$CeO_2/Al_2O_3$ was prepared by introducing $Ce(NO_3)_3 \cdot 6H_2O$ (Aldrich 99.99%) to the alumina by incipient wetness impregnation. The sample was calcined to 700°C for 2 h in air. The $CeO_2$ loading was 24 wt%.

$ZrO_2/CeO_2/Al_2O_3$ was prepared by sequential impregnation. $ZrO(NO_3)_2 \cdot nH_2O$ (Alfa Æsar, 99.99%) was impregnated onto the $CeO_2/Al_2O_3$ and the sample was calcined to 700°C for 2 h in air.

$CeO_2$–$ZrO_2/Al_2O_3$ *coimpregnated* was prepared by impregnating $Al_2O_3$ with a solution of $ZrO(NO_3)_2$ and $Ce(NO_3)_3$ and then calcining at 700°C for 2 h.

$CeO_2$–$ZrO_2$–$Al_2O_3$ *cogelled* was prepared by sol–gel synthesis. Aluminum isopropoxide was stirred in 2-methyl-2,4-pentanediol at 120°C to effect the substitution of the isopropoxy ligand by the diol. The end of evolution of isopropanol fume signaled completion of the substitution reaction. Then the beaker was cooled to 90°C and water (molar ratio $H_2O/Al = 10/1$) was added. Separately, a solution of cerium acetylacetonate hydrate (Aldrich) and zirconium acetylacetonate (98% Aldrich) in 2-propanol at 90°C was prepared. A small amount of $HNO_3$ was added to solubilize cerium acetylacetonate and the solution was stirred for 1 h, during which time controlled hydrolysis and condensation, brought about by the water in the cerium acetylacetonate hydrate ($Ce/H_2O = 1/6$), took place. Afterward, the contents of the two beakers were stirred together. The sample was then allowed to solidify and age at 90°C for 20 h while stirred. After filtering and drying at 100°C, the obtained powder was calcined to 700°C in flowing air in a procedure identical to the calcination of $Al_2O_3$.

The compositions and the BET surface areas of these samples are reported in Table 1. The samples thus obtained are referred to as fresh samples. Samples denoted R-$O_{25}$, R-$O_{550}$, and R-$O_{900}$were subjected to a redox treatment which consisted of $H_2$-TPR to 980°C followed by *in situ* oxidation with flowing oxygen at 25, 550, and 900°C for 2 h, respectively. Typically, 0.2 g of sample and 70 ml/min of $O_2$ were used. The sample denoted $CeO_2$–$ZrO_2$–$Al_2O_3O_{900}$ was prepared by calcination of corresponding fresh sample

**TABLE 1**

**Compositions and Surface Areas of Fresh Catalysts**

| Catalysts | Surface area ($m^2\ g^{-1}$) | Weight percent loading (ICP analysis) | | $Ce_xZr_{1-x}O_2/Al_2O_3$ (ICP analysis) |
|---|---|---|---|---|
| | | $CeO_2$ | $ZrO_2$ | |
| $ZrO_2/CeO_2/Al_2O_3$ | 142.3 | 21.8 | 13.2 | $Ce_{0.54}Zr_{0.46}O_2$ |
| $CeO_2$–$ZrO_2/Al_2O_3$ coimpregnated | 124.2 | 23.0 | 17.0 | $Ce_{0.49}Zr_{0.51}O_2$ |
| $CeO_2$–$ZrO_2$–$Al_2O_3$ cogelled | 169.3 | 23.3 | 20.7 | $Ce_{0.45}Zr_{0.55}O_2$ |
| $CeO_2$–$ZrO_2$–$Al_2O_3$ cogelled, 900°C | 138.8 | 23.3 | 20.7 | $Ce_{0.45}Zr_{0.55}O_2$ |

in air to 900°C for 2 h. The aged sample was prepared by heating a fresh sample in air at 1100°C for 5 h.

### 2.2. Sample Characterization

Temperature-programmed reduction (TPR) was conducted using a Hewlett–Packard 5890 gas chromatograph equipped with a TCD detector. A trap filled with molecular sieve and immersed in dry ice was placed before the detector. In a typical experiment, 200 mg of a sample was first heated in a flow (70 ml/min) of pure oxygen at 300°C for 30 min. After cooling to room temperature in $O_2$, the system was purged with Ar for 20 min. TPR was carried out by heating the sample at 10°C/min to 980°C in a 5% $H_2$–Ar mixture flowing at 30 ml/min. The TPR profile of the fresh samples may be somewhat distorted by the presence of absorbed species such as carbonates, as the pretreatment was only at 300°C. However, since the TPR of R-$O_{550}$ and R-$O_{900}$ samples were performed without exposing these samples to ambient air after the high temperature redox treatment, their reduction profiles should not be affected by any adsorbed species.

The chemical compositions of the samples were analyzed using a Thermo Jarrell Ash AtomScan25 spectrometer equipped with inductively coupled argon plasma emission source. The Sample (50–60 mg) was dissolved in 0.5 ml of 49% HF and then diluted with deionized water for the ICP analysis.

The X-ray powder diffraction (XRD) patterns were acquired with a Rigaku Geigerflex diffractometer operated at 40 kV and 20 mA with nickel-filtered Cu$K\alpha$ radiation. The samples were mounted on glass holders and the XRD patterns were recorded with a scanning speed of 1.2° (2θ) $min^{-1}$ with 0.1° step. In order to provide a more accurate (111) peak position for the ceria–zirconia solid solutions, a scanning speed of 0.04–0.15° (2θ) $min^{-1}$ was used over the 2θ range from 26 to 33°. The peak positions were calibrated using the Si(111) peak and the $LaB_6$ reference material ($a = 4.15680 \pm 0.00005$ Å, The Gem Dugout). The average particle size was calculated for the $Ce_xZr_{1-x}O_2(111)$ diffraction using the Scherrer equation (30).

Raman spectroscopy was performed using an Ar ion laser at 514.5 nm as an excitation source and a liquid-nitrogen-cooled CCD detector (Princeton Instruments). The laser power was 120 mW. The spectra of powder samples were taken at the ambient conditions. The BET surface areas were determined by $N_2$ adsorption using an Omnisorp 360 apparatus. The samples (about 0.1 g) were pretreated *in vacuo* at 250°C for 2 h for the BET measurements.

## 3. RESULTS

### 3.1. $H_2$ Temperature-Programmed Reduction

Figure 1 shows the $H_2$ TPR profile of a fresh sample of the sequentially impregnated $ZrO_2/CeO_2/Al_2O_3$ (curve a),

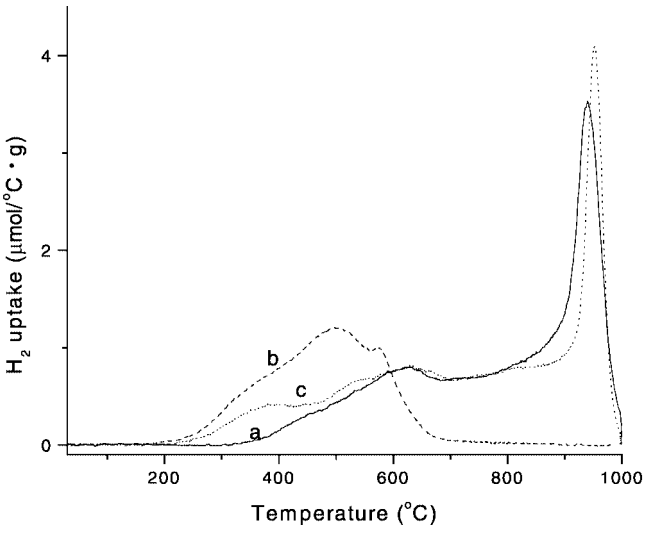


**FIG. 1.** TPR profiles of $ZrO_2/CeO_2/Al_2O_3$: (a) fresh, (b) R-$O_{550}$, and (c) R-$O_{900}$.

after R-$O_{550}$ (curve b), and after R-$O_{900}$ (curve c). These profiles were similar to those of $CeO_2/Al_2O_3$ after the respective treatments and differed from that of $ZrO_2/Al_2O_3$, which showed no $H_2$ consumption at all temperatures. The assignment of the reduction features of the fresh catalyst followed that described in the literature for $CeO_2/Al_2O_3$ (25–27): $H_2$ consumption below 700°C was ascribed to the reduction of dispersed ceria, and the uptake at 920°C to the reduction of large ceria crystallites with the concomitant formation of $CeAlO_3$ (20, 31, 32). For the R-$O_{550}$ sample (curve b), the $H_2$ consumption was absent above 700°C, while there was a significant increase in the amount of reducible ceria below 600°C and the emergence of a new reduction feature at ~350°C. Subjecting the R-$O_{550}$ sample to another cycle of R-$O_{900}$ resulted in the decrease of the low-temperature reduction peaks below 600°C and the reappearance of a high-temperature $H_2$ uptake peak (curve c), indicating significant reagglomeration of ceria. It is interesting that after the 900°C oxidative treatment, the catalyst still retained some low-temperature reducibility at 350°C.

Figure 2 shows the TPR profiles for $CeO_2$–$ZrO_2/Al_2O_3$ coimpregnated. Although the reduction peak positions were similar, their relative intensities were significantly different from that of the $CeO_2/ZrO_2/Al_2O_3$ sample prepared by sequential impregnation. For the fresh sample, the shoulder at 420°C was more pronounced and the peak at around 620°C was more intense, while the peak at 920°C was markedly reduced (curve a). The high-temperature peak at 920°C was absent for sample R-$O_{550}$ but appeared as a minor peak for sample R-$O_{900}$. That is, the R-$O_{900}$ sample, when compared to the fresh sample, had diminished high-temperature $H_2$ consumption and additional low-temperature reduction features.

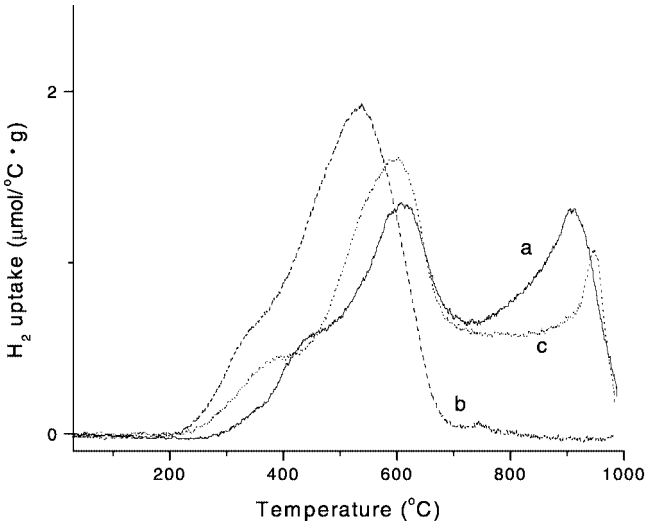


**FIG. 2.** TPR profiles of $CeO_2$–$ZrO_2$/$Al_2O_3$ coimpregnated: (a) fresh, (b) R-$O_{550}$, and (c) R-$O_{900}$.

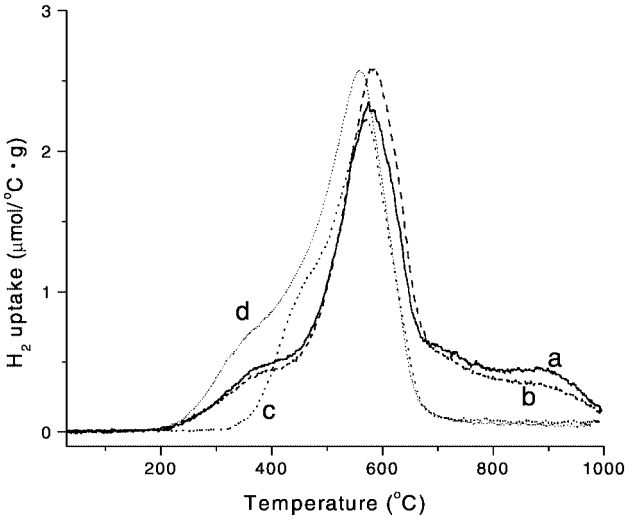


**FIG. 4.** TPR profiles of $O_{900}$ $CeO_2$–$ZrO_2$–$Al_2O_3$ cogelled after (a) one cycle of R-$O_{900}$ treatment, (b) four cycles of R-$O_{900}$, referred to as $(R\text{-}O_{900})_4$, (c) $(R\text{-}O_{900})_4$–R-$O_{25}$, and (d) $(R\text{-}O_{900})_4$–R-$O_{25}$–R-$O_{550}$.

For the $CeO_2$–$ZrO_2$–$Al_2O_3$ cogelled sample (Fig. 3), the fresh catalyst (curve a) showed intense $H_2$ uptake at 450 and 530°C and very little high-temperature $H_2$ consumption. As expected, after R-$O_{550}$, the low-temperature reducibility of the sample improved dramatically (curve b). Unlike the coimpregnated sample, after R-$O_{900}$, the cogelled sample became less reducible below 500°C than the fresh catalyst (compare Fig. 3, curves a and c). However, when compared to R-$O_{900}$ samples of other preparations, the reducibility below 700°C was still better. The reduction properties of the cogelled catalyst were also examined to see if the changes in response to thermal and redox treatments were reversible. It was found that identical reduction profiles of R-$O_{900}$ samples were obtained regardless of whether they originated from the fresh or the $O_{900}$ sample. The $H_2$ reduction profile of a sample that went through a R-$O_{550}$–R-$O_{900}$ cycle was also identical to that of one that simply went through a R-$O_{900}$ process.

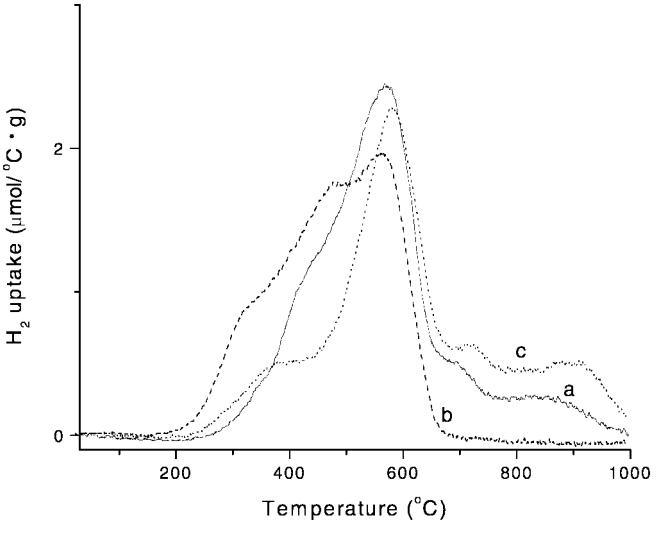


**FIG. 3.** TPR profiles of $CeO_2$–$ZrO_2$–$Al_2O_3$ cogelled: (a) fresh, (b) R-$O_{550}$, and (c) R-$O_{900}$.

Figure 4 shows that for a $O_{900}$ sample, the reduction profiles after one (Fig. 4, curve a) and four (Fig. 4, curve b) R-$O_{900}$ cycles were very similar. The latter sample, after TPR, was exposed to ambient atmosphere (henceforth referred to as the $(R\text{-}O_{900})_4$–R-$O_{25}$ sample) and was found to have been reoxidized to a significant extent, as indicated by its $H_2$ TPR profile (Fig. 4, curve c). The $(R\text{-}O_{900})_4$–R-$O_{25}$ sample was subjected to another R-$O_{550}$ cycle, and its reduction profile (Fig. 6, curve d) looked distinctly different from that of a R-$O_{900}$ sample and bore a much closer resemblance to that of a R-$O_{550}$ sample (Fig. 3, curve b).

Table 2 summarizes the $H_2$ uptakes of the various catalysts studied. From the $H_2$ uptakes and assuming that the reduction occurs as

$$2CeO_2 + H_2 = Ce_2O_3 + H_2O,$$

the percentage of Ce(IV) reduced to Ce(III) was calculated. For the fresh samples, not all of the ceria was reduced even after reduction to 980°C. $CeO_2$/$Al_2O_3$ and $ZrO_2$/$CeO_2$/$Al_2O_3$ had the highest fraction of reducible ceria, whereas the cogelled and coimpregnated samples had notably higher fractions of ceria that can be reduced below 700°C. In fact, the fraction of reducible $Ce^{4+}$ below 700°C for the cogelled preparation was more than twice that of the sequentially impregnated sample. The $H_2$ uptake data of R-$O_{550}$ samples showed that 550°C was insufficient to fully reoxidize the reduced ceria. However, a significantly larger fraction of ceria was reoxidized for the coimpregnated and cogelled samples than for the other preparations. It is

**TABLE 2**

**Summary of $H_2$-TPR Results**

| Sample | $H_2$ uptake (μ mol/g)[a] | |
|---|---|---|
| | Below 980°C | Below 700°C |
| 24% $CeO_2/Al_2O_3$ | | |
| Fresh | 607.0 (87.0) | 207.0 (29.7) |
| R-$O_{550}$ | 379.0 (54.4) | 379.0 (54.4) |
| R-$O_{900}$ | 581.5 (83.6) | 235.0 (33.8) |
| $ZrO_2/CeO_2/Al_2O_3$ | | |
| Fresh | 535.5 (85.0) | 173.0 (27.4) |
| R-$O_{550}$ | 281.0 (44.6) | 281.0 (44.6) |
| R-$O_{900}$ | 523.5 (81.4) | 221.5 (34.5) |
| Coimpregnated $CeO_2$–$ZrO_2/Al_2O_3$ | | |
| Fresh | 557.0 (80.6) | 292.5 (42.3) |
| R-$O_{550}$ | 441.5 (63.9) | 436.5 (63.2) |
| R-$O_{900}$ | 545.5 (79.0) | 354.5 (51.3) |
| Cogelled $CeO_2$–$ZrO_2$–$Al_2O_3$ | | |
| Fresh | 569.0 (81.3) | 504.0 (72.0) |
| R-$O_{550}$ | 510.5 (72.9) | 509.5 (72.8) |
| R-$O_{900}$ | 533.0 (76.2) | 411.0 (58.7) |
| Aged | 540.0 (77.2) | 341.1 (48.7) |
| Aged-R-$O_{550}$ | 523.0 (74.8) | 441.8 (63.1) |

[a] Numbers in parentheses show fraction (percentage) of Ce reduced. Calculated based on total Ce content in the samples.

interesting that for a $CeO_2$–$ZrO_2$–$Al_2O_3$ cogelled, most of the reoxidation of $Ce^{3+}$ generated during TPR took place at 25°C (57.8%, as calculated from the TPR data shown in Fig. 4, curve c) and increasing the temperature to 900°C reoxidized 93.7% of the $Ce^{3+}$. The reduction profile of this room-temperature reoxidized sample, however, lacked the low-temperature reduction shoulder prominent in the sample reoxidized at 550°C (Fig. 3, curve b). After R-$O_{900}$, the fraction of reducible Ce below 700°C was on the order of $CeO_2$–$ZrO_2$–$Al_2O_3$ > $CeO_2$–$ZrO_2/Al_2O_3$ > $ZrO_2/CeO_2/Al_2O_3 \simeq CeO_2/Al_2O_3$.

### 3.2. XRD

Figure 5A compares the XRD patterns of the fresh samples and Fig. 5B compares the position of their (111) diffractions. For Fig. 5B, the peak positions were calibrated by comparison with another scan of the sample mixed with a silicon standard. The γ-$Al_2O_3$ diffraction pattern was very broad, but its most intense peak, at $2\theta = 66.8°$, was observed for all samples. The patterns of $ZrO_2/CeO_2/Al_2O_3$ and $CeO_2/Al_2O_3$ were those of cubic $CeO_2$. For the former sample, the position of its (111) diffraction indicated no formation of any solid solution between ceria and zirconia, but at the same time no $ZrO_2$ diffraction peaks were detected. $Ce_xZr_{1-x}O_2$ mixed oxides were formed by the coimpregnation and cogelation methods, as indicated by the shift of the (111) peaks to higher angles. $CeO_2$–$ZrO_2$–$Al_2O_3$ cogelled appeared to be a single phase, as the (111) diffraction peaks at $2\theta = 29.26°$ can be fitted with a single Gaussian curve. The chemical composition of the mixed oxide phase was estimated to be $Ce_{0.55}Zr_{0.45}O_2$ according to Fig. 6. The plot was constructed using data compiled from the JCPDS database (33). The $CeO_2$–$ZrO_2/Al_2O_3$ coimpregnated sample appeared to consist of two phases (Fig. 5B, curve c). The major phase was a solid solution of the composition $Ce_{0.7}Zr_{0.3}O_2$ (diffraction peak at $2\theta = 28.87°$) while the minor phase was $ZrO_2$ rich ($2\theta = 29.99°$). The peak intensities of the cogelled and coimpregnated samples were much weaker than those of the sequential impregnated sample and $CeO_2/Al_2O_3$, suggesting either a higher dispersion or a higher degree of disorder of the mixed oxides phase.

After R-$O_{550}$, no $CeO_2$ diffraction peak was detected for $CeO_2/Al_2O_3$ and $ZrO_2/CeO_2/Al_2O_3$ (Fig. 7, curves a and b,

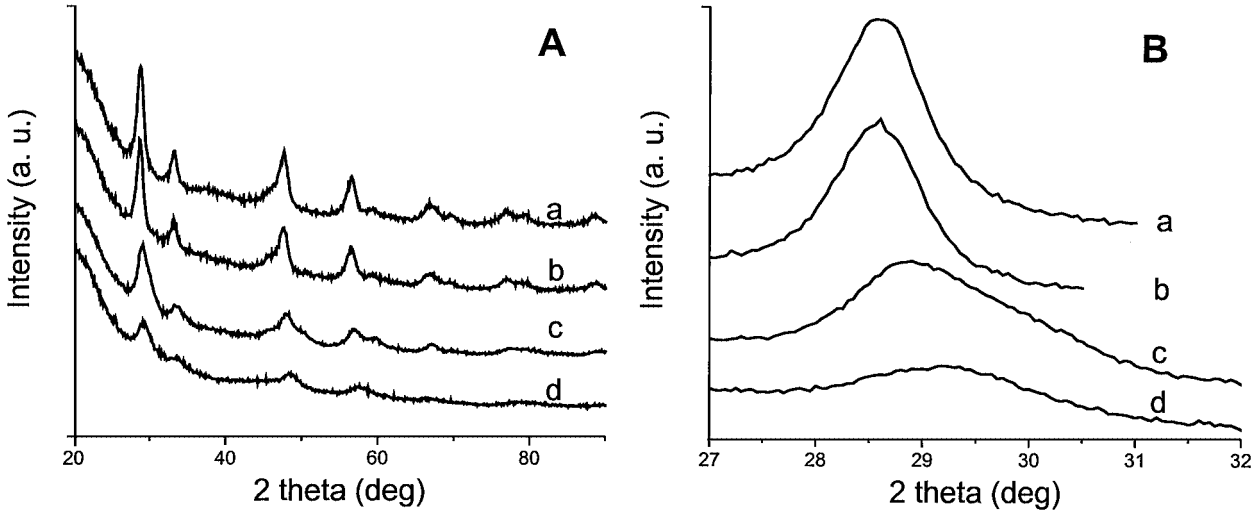


**FIG. 5.** XRD patterns of fresh samples: (a) 24% $CeO_2/Al_2O_3$, (b) $ZrO_2/CeO_2/Al_2O_3$, (c) $CeO_2$–$ZrO_2/Al_2O_3$, and (d) $CeO_2$–$ZrO_2$–$Al_2O_3$ at 2θ range of 20–90° (A) and 27–32° (B).

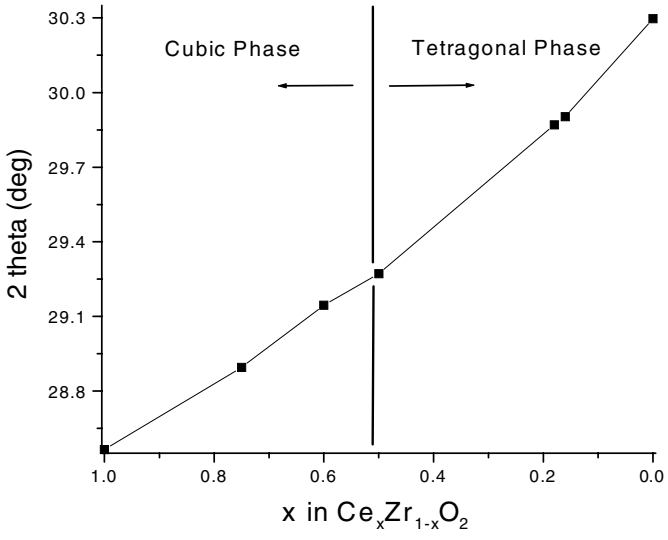


**FIG. 6.** Position of the XRD (111) reflection of $Ce_xZr_{1-x}O_2$ versus Ce content.

respectively). Peaks at $2\theta = 33.5$, 41.5, and 54.5° indicated the presence of $CeAlO_3$. An additional diffraction peak at 30.6° and a shoulder at 31.1° were also observed for $CeO_2/ZrO_2/Al_2O_3$. These latter peaks, although shifted by 0.3°, were consistent with the presence of tetragonal $ZrO_2$. For $CeO_2$–$ZrO_2/Al_2O_3$ coimpregnated, the XRD peaks had broadened. In fact, the width and asymmetry of the (111) peak suggested that phases of compositions ranging from pure $CeO_2$ ($2\theta = 28.5°$) to pure $ZrO_2$ ($2\theta = 30.3°$) were present (curve c). In contrast, after R-$O_{550}$, the peak intensities were increased, the peak widths were narrowed, and the peak positions were shifted toward higher angles for $CeO_2$–$ZrO_2$–$Al_2O_3$ cogelled (curve d).

Table 3 summarizes the XRD parameters and information deduced from the (111) diffraction peak of $CeO_2$–$ZrO_2$–$Al_2O_3$ cogelled after various treatments. It is interesting that little increase in particle size, i.e., little sintering of the crystalline portion of the mixed oxide, was observed even after severe redox treatments. On the other hand, the temperature and redox atmosphere of treatments affected both the amount of crystalline $Ce_xZr_{1-x}O_2$ phase and its composition. Assuming that the (111) peak area of the 900°C oxidized sample represents all of the $Ce_xZr_{1-x}O_2$ present, the percentage of XRD-detectable $Ce_xZr_{1-x}O_2$ was 32, 59, 64, and 100% for fresh, R-$O_{25}$, R-$O_{550}$, and R-$O_{900}$ samples, respectively. It appeared that high-temperature treatment in an oxidative atmosphere favored ordering of the crystalline phase. The phase compositions of $Ce_xZr_{1-x}O_2$ were estimated from the positions of the (111) peak using the plot shown in Fig. 6. For the $O_{900}$ sample, the composition was the same as that determined from ICP analysis. On the other hand, the $Ce_xZr_{1-x}O_2$ phase of all other samples after redox treatment was enriched in Zr relative to the bulk composition, with the largest enrichment found in samples R-$O_{25}$ and R-$O_{550}$.

### *3.3. Raman Spectroscopy*

Figure 8 compares the Raman spectra of the fresh, R-$O_{550}$, R-$O_{900}$, and $O_{900}$ samples of $CeO_2$–$ZrO_2$–$Al_2O_3$ cogelled. The spectra of the fresh sample suggested that it was the *t″* phase, as it had an intense band at 465 $cm^{-1}$ and a small band at 310 $cm^{-1}$ (26). An additional broad feature centered at about 640 $cm^{-1}$could be ascribed to a defect structure induced by introducing Zr into the fluorite structure of $CeO_2$ (26). Heating of $CeO_2$–$ZrO_2$–$Al_2O_3$ at

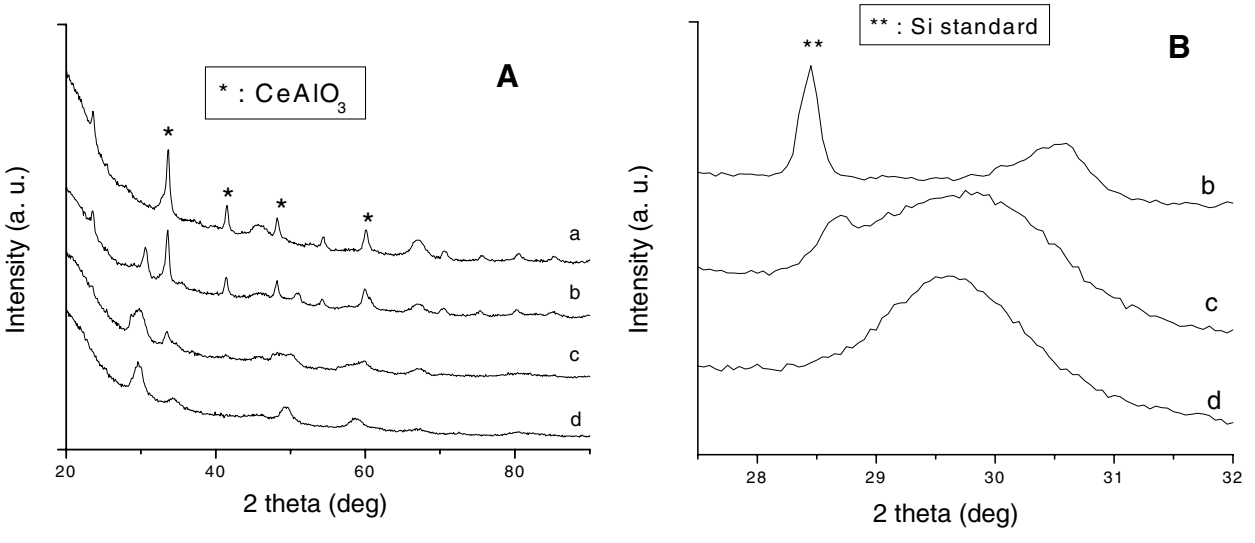


**FIG. 7.** XRD patterns of samples after R-$O_{550}$ treatment: (a) 24% $CeO_2/Al_2O_3$, (b) $ZrO_2/CeO_2/Al_2O_3$, (c) $CeO_2$–$ZrO_2/Al_2O_3$, and (d) $CeO_2$–$ZrO_2$–$Al_2O_3$ at $2\theta$ range of 20–90° (A) and 27–32°(B).

**TABLE 3**

**Composition, Average Particle Size, and X-Ray-Detectable Fraction of the $Ce_xZr_{1-x}O_2$ Phase in the $CeO_2$–$ZrO_2$–$Al_2O_3$ Cogelled Samples**

| | $Ce_xZr_{1-x}O_2$ | | | | |
|---|---|---|---|---|---|
| Pretreatment | $2\theta^\circ$ | Relative integrated intensity of (111) diffraction | Composition of crystalline fraction[a] | Particle size (nm) | XRD-detectable fraction[b] (%) |
| Fresh | 29.26 | 17.8 | $Ce_{0.55}Zr_{0.45}O_2$ | 5.4 | 32 |
| $O_{900}$ | 29.35 | 55.2 | $Ce_{0.45}Zr_{0.55}O_2$ | 6.1 | 100 |
| R-$O_{25}$ | 29.58 | 32.6 | $Ce_{0.35}Zr_{0.65}O_2$ | 6.3 | 59 |
| R-$O_{550}$ | 29.59 | 35.3 | $Ce_{0.35}Zr_{0.65}O_2$ | 6.4 | 64 |
| R-$O_{900}$ | 29.46 | 55.2 | $Ce_{0.40}Zr_{0.60}O_2$ | 6.5 | 100 |

[a] Deduced from the position of the (111) diffraction (Fig. 10 B).
[b] Calculated from the (111) diffraction intensity, assuming that 100% of $Ce_xZr_{1-x}O_2$ was XRD detectable in the $O_{900}$ sample.

900°C (samples R-$O_{900}$ and $O_{900}$) resulted in a significant increase in intensity of the peak at 465 $cm^{-1}$. The spectrum of R-$O_{550}$ sample was almost featureless, showing very weak and broad peaks at 640, 602, 455, and 306 $cm^{-1}$.

### *3.4. Accelerated Aging of Cogelled $CeO_2$–$ZrO_2$–$Al_2O_3$*

The properties of the cogelled sample after further thermal treatment of 1100°C for 5 h were characterized by XRD and TPR. Some minor compositional inhomogeneity had resulted, as indicated by the broadening of the (111) diffraction peak (Fig. 9B, curve a). A single gaussian peak still represents this peak well. Another indication of some phase segregation was the splitting of the peak at around 49° (Fig. 9A, curve a). The alumina support remained in the γ form. After R-$O_{550}$ treatment, there was no evidence of $CeAlO_3$ formation (Fig. 9a, curve b). The TPR profile of this aged sample was shifted to a higher temperature. However, after a R-$O_{550}$ treatment, some improved reducibility was again observed, albeit the $H_2$ uptake peaks were still at a higher temperature than the R-$O_{550}$ of the fresh sample. Total $H_2$ consumption and $H_2$ consumption below 700°C is shown in Table 2.

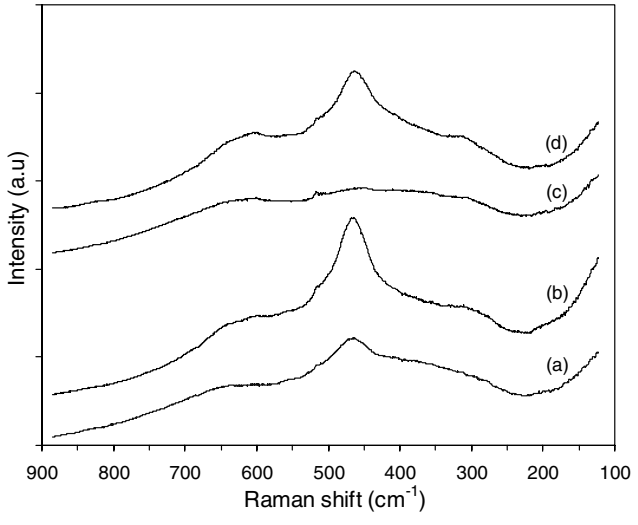


**FIG. 8.** Raman spectra of the cogelled $CeO_2$–$ZrO_2$–$Al_2O_3$ samples: (a) fresh, (b) $O_{900}$, (c) R-$O_{550}$, (d) R-$O_{900}$.

## 4. DISCUSSION

The TPR and XRD results clearly show that the reduction properties and the composition and phases of $Ce_xZr_{1-x}O_2$ depend on both the methods of preparation and the pretreatment. The cogelled preparation procedure was designed to maximize the interaction between ceria and zirconia. Condensation of the acetylacetonate precursors of cerium and zirconium was allowed to proceed before mixing with the partially hydrolyzed aluminum precursor. In order to ensure the formation of small clusters of $CeO_2$–$ZrO_2$ on $Al_2O_3$, the prehydrolysis and condensation of the precursors of cerium and zirconium were controlled by limiting the time and the amount of water. The addition of the chelating agent, 2-methyl-2,4-pentanediol, moderated the hydrolysis rate of aluminum isopropoxide and made it comparable to the hydrolysis rates of the other two components. In addition, it was previously shown that the addition of 2-methyl-2,4-pentanediol to the synthesis solution resulted in the formation of $Al_2O_3$ of unusual thermal stability (28). The advantageous results of using this synthesis method rather than the more conventional impregnation are discussed below.

As solid solution of $Ce_xZr_{1-x}O_2$ was not formed in the sequentially impregnated sample, its physical and redox properties were very similar to those of $CeO_2/Al_2O_3$. The strong interaction between $ZrO_2$ and $Al_2O_3$, attested to by the absence of XRD-detectable $ZrO_2$, even after heating to 900°C in air, is the underlying reason for the failure to form the mixed oxide. Multiple phases of $Ce_xZr_{1-x}O_2$ were

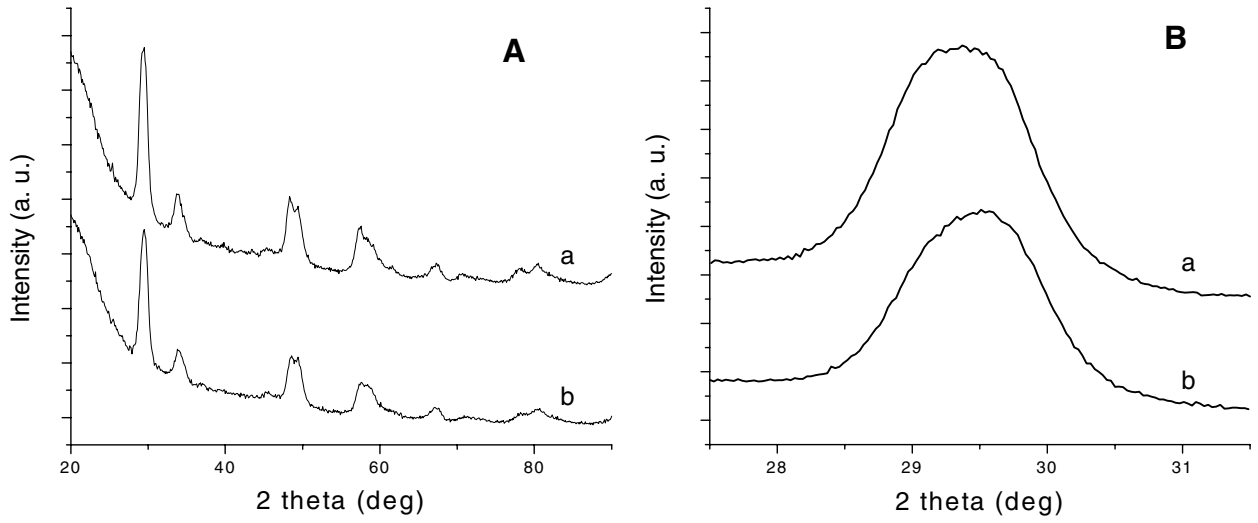


**FIG. 9.** XRD patterns of $CeO_2$–$ZrO_2$–$Al_2O_3$ samples: (a) after calcination at 1100°C for 5 h and (b) followed by R-$O_{550}$ treatment at 2θ range of 20–90° (A) and 27.5–31.5°(B).

present in the fresh coimpregnated sample and the inhomogeneity increased with redox treatment at high temperatures. These results are in agreement with other reports of $Ce_xZr_{1-x}O_2/Al_2O_3$ samples of intermediate Zr contents prepared by the coimpregnation method. These samples also had difficulty maintaining a single homogeneous phase after high-temperature treatment (19, 22–34).

The cogelled method resulted in stabilizing the particle size of the $Ce_xZr_{1-x}O_2$. Table 3 shows that the particles size of the fresh catalyst only increased from 5.4 to 6.5 nm after it was subjected to the R-$O_{900}$ treatment. The catalyst was single phase and homogeneous after 900°C calcinations, and the (111) XRD peak was symmetrical and could be fitted with a single Gaussian curve after five redox cyclings. In contrast, the widely studied $Ce_xZr_{1-x}O_2$ synthesized by Rhodia, after three redox cyclings, showed compositional inhomogeneity, as evidenced by the asymmetry of the (111) peak (15). The laser Raman spectra of the fresh, $O_{900}$, and R-$O_{900}$ samples resembled that of the $t''$ phase spectra of Yashima *et al.* (26). The oxygen in the $t''$ polymorph is displaced from the ideal fluorite sites, and this form of $Ce_xZr_{1-x}O_2$ is generally known as a pseudo cubic phase of the Fm3m space group (4). Although, the $t''$ phase is found in the compositional range of 65–80 mol% of $CeO_2$, Fornasiero *et al.* (4) synthesized $Ce_{0.5}Zr_{0.5}O_2$ of $t''$ phase that was stable at 500°C. They observed that the stabilization of this cubic form at 500°C at such low Ce content was significant and that it was possibly due to the small particle size of their preparation. Upon heating to 800°C, tetragonalization of their mixed oxide took place. In our cogelled sample, the cubic phase was retained even after heating to 900°C and we suggest that the resistance of this sample to phase transform is due to its ability to retain its small crystallite size.

After 1100°C treatment, minor phase and compositional segregation occurred. The (111) peak broadened but still could be fitted reasonably well with a single Gaussian curve. Di Monte *et al.* (23) reported that after the same thermal treatment, their coimpregnated $Ce_{0.6}Zr_{0.4}O_2/Al_2O_3$ had disproportionated into a ceria-rich phase (74%) and a zirconia-rich phase (26%). More important still, they observed $CeAlO_3$ formation after the sample was subjected to reduction and oxidation treatment. On the other hand, the XRD spectrum of the aged cogelled sample after R-$O_{550}$ treatment showed no formation of $CeAlO_3$ (Fig. 9A, curve b). This is significant because formation of $CeAlO_3$ leads to loss of OSC. Complete transformation of γ- to θ-$Al_2O_3$ had taken place in the Di Monte preparations whereas no significant trace of any minor alumina phase was detected in our cogelled preparation. The structural stability of this preparation translated into good redox properties and the $H_2$ consumption below 700°C of the aged-R–$O_{550}$ sample was 87.6% of the fresh catalyst calcined at 700°C (Table 2).

All R-$O_{550}$ samples showed marked enhancement in the low-temperature reducibility relative to the fresh sample, as shown by the TPR profiles. This improved low-temperature reducibility was especially prominent in the cogelled sample. For the fresh cogelled sample, the $H_2$ consumption above 700°C probably arises from large crystallites of $CeO_2$ and $Ce_xZr_{1-x}O_2$. Reduction below 700°C is due to both the crystalline and amorphous phases, as the total $H_2$ consumption below 700°C represented 72% of the total $Ce^{4+}$ while the crystalline phase was only 32% of the total mixed oxide. $H_2$ consumption below 700°C can be deconvoluted into three peaks, centered around 410, 491, and 577°C; the peak positions are remarkably similar to those observed for the unsupported $Ce_{0.5}Zr_{0.5}O_2$ prepared

by Fornasiero *et al.* (4). After their assignment, the 410°C peak is assigned to the reduction of surface region,while the peaks at 491 and 577°C are assigned to the reduction of the bulk of the mixed oxide. After the R-$O_{550}$ process, there was a new $H_2$ uptake peak, at 320°C, and the $H_2$ consumption at 410 and 490°C was increased while that at 577°C decreased.

Concomitant with the enhanced reducibility is a change in the chemical composition of the crystalline phase, as indicated by XRD. The fresh cogelled sample consists of a crystalline phase of $Ce_{0.55}Zr_{0.45}O_2$ and an amorphous phase somewhat enriched in Zr. After the R-$O_{550}$ process, XRD spectra indicated significant enrichment of Zr in the crystalline phase (now ~64% of the total mixed oxide) to yield a composition of $Ce_{0.35}Zr_{0.65}O_2$. Similar changes in composition had been reported for reduced $Ce_xZr_{1-x}O_2$ supported on $Al_2O_3$ by Yao *et al.* (19). They attributed this change to the assimilation of unincorporated $ZrO_2$ of the fresh sample into the mixed oxide upon reductive treatment. Our study of the sequentially impregnated sample showed that $ZrO_2$, not initially incorporated into the solid solution, interacted with $Al_2O_3$ strongly and redox treatment could not induce its incorporation into the $Ce_xZr_{1-x}O_2$ solid solution. Thus the observed compositional change must be due to the formation of XRD-silent Ce species.

There is a large disparity in the ionic radii between $Ce^{3+}$ (1.1 Å), $Ce^{4+}$ (0.97 Å), and $Zr^{4+}$ (0.84Å), and partial segregation of $Ce^{3+}$ to the surface can occur because the crystal lattice of $Ce_xZr_{1-x}O_2$ cannot easily accommodate its larger size. Upon reoxidation, the segregated Ce cations form small ceria-rich clusters on top of the mixed oxide, which is now richer in Zr. Reduction of the surface and the bulk of this new ceria-rich phase is probably responsible for the enhanced reducibility at 320 and 410°C. The assignment of the reduction peaks is consistent with the fact that, in general, the onset of $H_2$ consumption is at lower temperatures for mixed oxides rich in ceria (15). The low level of $H_2$ uptake at 320°C suggests that the amount of these newly generated ceria-rich clusters is not large and is consistent with the small difference between the chemical composition of the fresh and R-$O_{550}$ samples. That this new phase is in intimate contact with the crystalline mixed oxide is seen by the fact that oxidation of the reduced sample at higher temperatures (sample R-$O_{900}$) showed significant reintegration of ceria into the crystalline phase and concomitant reduced $H_2$ consumption around 320°C. It is also supported by the fact that no $CeAlO_3$ XRD peaks were detected after redox treatments. The fact that this phenomenon of compositional change was not reported for the unsupported, large crystallites of the mixed oxide may be due to two reasons. First, the same surface coverage of the segregated Ce would correspond only to a small change in the bulk of a large particle, but to a much larger change in the crystalline composition of a small particle. Second, the high surface area of the mixed oxide particles in the cogelled preparation is better able to support the dispersed ceria-rich phase.

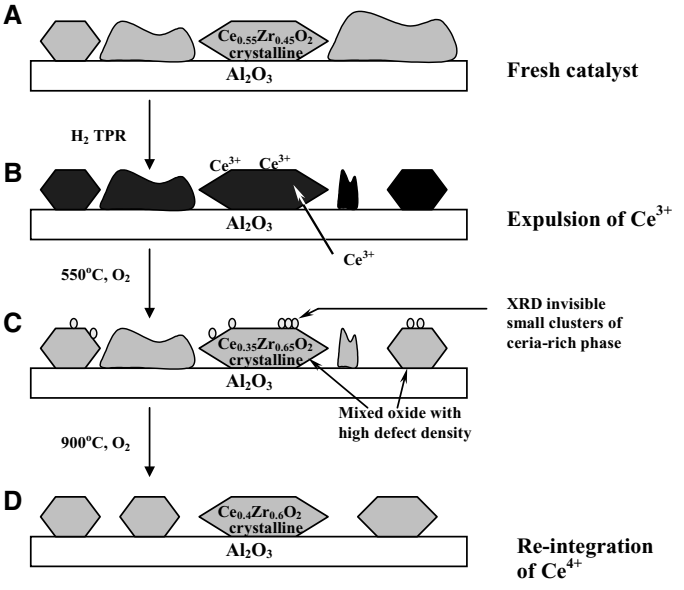


**FIG. 10.** Schematic representation of changes of the cogelled $CeO_2$–$ZrO_2$–$Al_2O_3$ sample during the redox process.

Laser Raman spectrum of the R-$O_{550}$ sample is quite attenuated. The attenuation is not due to tetragonalization because the Raman spectra of the R-$O_{900}$ sample, similar to that of the fresh sample, is that of a $t''$ phase which is thermodynamically less stable than the tetragonal phase for this composition of $Ce_xZr_{1-x}O_2$. The attenuation may result from a high concentration of defect sites generated by the reduction. This is consistent with the relative changes in the reduction behavior of the bulk mixed oxide: an increase in the 491°C relative to the 577°C TPR peak. After annealing at 900°C, as in the R-$O_{900}$ sample, the predominant $H_2$ uptake was at 577°C. The compositional and redox changes that accompanied redox and thermal treatments as described above are summarized pictorially in Fig. 10.

## 5. CONCLUSIONS

Preparation procedures that promote a high degree of interaction between ceria and zirconia to form $Ce_xZr_{1-x}O_2/Al_2O_3$ result in samples that exhibit redox properties highly favorable for use in the three-way catalysts. The intimate interaction between ceria and zirconia also retards the formation of $CeAlO_3$ during reduction. Cogelation appears to be the most effective method to facilitate such intimate interaction. It results in a Zr-rich cubic ($t''$ phase) mixed oxide, which is stable to 900°C without segregation of the components. This supported mixed oxide is also highly resistant to sintering when subjected to redox cycles.

The redox properties of all $Ce_xZr_{1-x}O_2/Al_2O_3$ samples can be modified by a reduction–oxidation treatment and the most pronounced modification is observed for the co-gelled sample. There are two different aspects to the enhanced reducibility with a R-$O_{550}$ process. A new, very-low-temperature $H_2$ uptake peak was observed, which we propose to be due to the reduction of very small particles of ceria-rich phase resting on the surface of larger crystallites of bulk oxides. The formation of this ceria-rich phase during redox process is promoted by the large disparity in ionic radii between $Ce^{3+}$ and $Zr^{4+}$. Besides this new low-temperature feature, there is a general enhancement in the reducibility below 700°C, which is due to an increase in defect site density caused by the disruption of the bulk oxide structure during reduction and this is observed in both the bulk and the supported $Ce_xZr_{1-x}O_2$.

## ACKNOWLEDGMENTS

Financial support for this project was provided by the Coordinating Council Research Inc. We thank Johnson Matthey for providing a $CeO_2$-$ZrO_2$ sample for XRD calibration.

## REFERENCES

1. Trovarelli, A., *Catal. Rev.–Sci. Eng.* **38**, 439 (1996).
2. Taylor, K. C., *Catal. Rev.–Sci. Eng.* **35**, 457 (1993).
3. Farrauto, R. J., and Heck, R. M., *Catal. Today* **51**, 351 (1999).
4. Fornasiero, P., Balducci, G., Di Monte, R., Kašpar, J., Sergo, V., Gubitosa, G., Ferrero, A., and Graziani, M., *J. Catal.* **164**, 173 (1996).
5. Di Monte, R., Fornasiero, P., Kašpar, J., Rumori, P., Gubitosa, G., and Graziani, M., *Appl. Catal. B* **24**, 157 (2000).
6. Pijolat, M., Prin, M., Soustelle, M., Touret, O., and Nortier, P., *J. Chem. Soc. Faraday Trans.* **91**, 3941 (1995).
7. Fornasiero, P., Fonda, E., Di Monte, R., Vlaic, G., Kašpar, J., and Graziani, M., *J. Catal.* **187**, 177 (1999).
8. Vlaic, G., Fornasiero, P., Geremia, S., Kaspar, J., and Graziani, M., *J. Catal.* **168**, 386 (1997).
9. Lemaux, S., Bensaddik, A., van der Eerden, A. M. J., Bitter, J. H., and Koningsberger, D. C., *J. Phys. Chem.* **B105**, 4810 (2001).
10. Trovarelli, A., Zamar, F., Llorca, J., de Leitenburg, C., Dolcetti, G., and Kiss, J. T., *J. Catal.* **169**, 490 (1997).
11. Fornasiero, P., Di Monte, R., Rango, R. G., Kašpar, J., Meriani, S., Trovarelli, A., and Graziani, M., *J. Catal.* **151**, 168 (1995).
12. Nunan, J., and Borton, A., Abstr. Pap. *Am. Chem. Soc.* **219** (CATL-2), 36 (2000).
13. Balducci, G., Fornasiero, P., Di Monte, R., Kašpar, J., Meriani, S., and Graziani, M., *Catal. Lett.* **33**, 193 (1995).
14. Vidal, H., Kašpar, J., Pijolat, M., Colon, G., Benal, S., Cordón, A., Perrichon, V., and Fally, F., *Appl. Catal. B* **27**, 49 (2000).
15. Vidal, H., Kašpar, J., Pijolat, M., Colon, G., Bernal, S., Cordón, A., Perrichon, V., and Fally, F., *Appl. Catal. B* **30**, 75 (2001).
16. Fally, F., Perrichon, V., Vidal, H., Kašpar, J., Blanco, G., Pintado, J. M., Bernal, S., Colon, G., Daturi, M., and Lavalley, J. C., *Catal. Today* **59**, 373 (2000).
17. Kung, D. H., and Kung, M. C., unpublished results.
18. Fernandez-Garcia, M., Martinez-Arias, A., Iglesias-Juez, A., Belver, C., Hungria, A. B., Conesa, J. C., and Soria, J., *J. Catal.* **194**, 385 (2000).
19. Yao, M. H., Baird, R. J., Kunz, F. W., and Hoost, T. E., *J. Catal.* **166**, 67 (1997).
20. Shyu, J. Z., Weber, W. H., and Gandhi, H. S., *J. Phys. Chem.* **92**, 4964 (1988).
21. Miki, T., Ogawa, T., Ueno, A., Matsuura, S., and Santo, M., *Chem. Lett.* 565 (1998).
22. Di Monte, R., Fornasiero, P., Kašpar, J., Graziani, M., Gatica, J. M., Beanla, S., and Gomez-Herrero, A., *Chem. Commun.* 2167 (2000).
23. Di Monte, R., Fornasiero, P., Kašpar, J., and Graziani, M., *Stud. Surf. Sci. Catal.* **140**, 229 (2001).
24. Yashima, M., Morimoto, K., Ishizawa, N., and Yoshimura, M., *J. Am. Ceram. Soc.* **76**, 1745 (1993).
25. Yashima, M., Morimoto, K., Ishizawa, N., and Yoshimura, M., *J. Am. Ceram. Soc.* **76**, 2865 (1993).
26. Yashima, M., Arashi, H., Kakihana, M., and Yoshimura, M., *J. Am. Ceram. Soc.* **77**, 1067 (1994).
27. Kašpar, J., Fornasiero, P., and Graziani, M., *Catal. Today* **50**, 285 (1999).
28. Maeda, K., Mizukami, F., Niwa, S., Watanabe, M., Toba, M., and Masuda, K., *J. Chem. Soc. Faraday Trans.* **88**, 97 (1992).
29. Yan, J. Y., Kung, M. C., Sachtler, W. M. H., and Kung, H. H., *J. Catal.* **172**, 178 (1997).
30. Thomas, J. M., and Thomas, W. J., "Principles and Practice of Heterogeneous Catalysis." VCH, Weinheim/New York, 1996.
31. Yao, H. C., and Yao, Y. F. Y., *J. Catal.* **86**, 254 (1984).
32. Piras, A., Trovarelli, A., and Dolcetti, G., *Appl. Catal. B* **28**, L77 (2000).
33. JCPDS files: 43-1002, 28-0271, 38-1439, 38-1436, 80-0785, 38-1437, 88-1007.
34. Di Monte, R., Fornasiero, P., Kašpar, J., Ferrero, A., Gubitosa, G., and Graziani, M., *Stud. Surf. Sci. Catal.* **116**, 559 (1998).